In situ fabricating Rh/Ga_2O_3 photothermal catalyst for dry reforming of methane

Yuqiao Li [a], Dezheng Li [a], Huimin Liu [a*], Yiming Lei [a,b*], Rongda Zhao [c*], Dehua He [d] Ze Zheng [a], Hui Luo [a], Aidi Liu [a]

[a], School of Chemical and Environmental Engineering, Liaoning University of Technology, Jinzhou 121001, China

[b], Department of Chemistry, Universitat Autònoma de Barcelona, Cerdanyola del Vallès, Barcelona 08193, Spain

[c], School of Materials Science and Engineering, Liaoning University of Technology, Jinzhou 121001, China

[d], Innovative Catalysis Program, Key Lab of Organic Optoelectronics & Molecular Engineering of Ministry of Education, Department of Chemistry, Tsinghua University, Beijing 100084, China

Table S1. Surface area and average pore size of Ga_2O_3, 1% Rh_2O_3/Ga_2O_3, ZnO, and 1% Rh_2O_3/ZnO.

Catalysts	Surface area ($m^2 \cdot g^{-1}$)	Average pore size (nm)
Ga_2O_3	3.9	19.1
1% Rh_2O_3/Ga_2O_3	4.6	21.4
ZnO	4.3	7.8
1% Rh_2O_3/ZnO	1.5	17.4

Table S2. The conversion rates of CO_2 and CH_4 were compared with other studies

Catalyst	Reaction conditions	Catalytic performance ($\mu mol\ g^{-1}\ min^{-1}$)		Stability (h)	Source
		CO_2	CH_4		
Rh/Ga_2O_3	Photothermal	112	76.3	4	This work
$Pt\text{-}Au/SiO_2$	Photothermal	68.6	54.5	1	1
$Ni@SiO_2$-yolk	Photothermal	510	480	5	2
$Cu_{19.8}Ru_{0.2}$	Photothermal	n.m	4.6	20	3
NiO_x	Thermal	12.8	17.1	20	4
$15Ni/Al_2O_3$	Photothermal	38.5	46.9	5	5
Rh-Au/SBA-15	Photothermal	60	53.3	8	6
Rh/Al_2O_3	Thermal	n.m	0.6	0.8	7
$Co\text{-}Ce/ZrO_2$	Thermal	1.7	1.5	6	8
$Pd_{90}Au_{10}/Al_2O_3$	Photothermal	1210.6	930.3	0.5	9
10%Rh/STO	Photothermal	2.6	2.6	13	10

Note: n.m means not mentioned

Table S3. ICP-OES detects Rh content.

Catalyst	Rh loading (wt%)
Ga_2O_3	-
Rh_2O_3/Ga_2O_3	0.70
ZnO	-
Rh_2O_3/ZnO	0.86

Table S4. DRM catalytic performance of 1% Rh/Ga_2O_{3-x} and 1% Rh/ZnO_{1-x} under photothermal, thermal, and light conditions.

Catalysts	Reaction condition	Reactant	Conversion (μmol $g^{-1}min^{-1}$)
1% Rh/Ga_2O_{3-x}	Photothermal	CO_2	112
		CH_4	76.3
	Thermal	CO_2	71.9
		CH_4	60.4
	Light	CO_2	0
		CH_4	0
1% Rh/ZnO_{1-x}	Photothermal	CO_2	50.8
		CH_4	39.3
	Thermal	CO_2	49.9
		CH_4	39.3
	Light	CO_2	0
		CH_4	0

Photothermal reaction conditions: CH_4 : CO_2 = 1 : 1, total flow rate: 10 mL min^{-1}, catalyst 0.094 g, reaction time 30 min, reaction temperature 500 °C, 300 W Xe lamp.

Thermal reaction conditions: CH_4 : CO_2 =1 : 1, total flow rate: 10 mL min^{-1}, catalyst 0.094 g, reaction time 30 min, reaction temperature 500 °C.

Light reaction conditions: CH_4 : CO_2 = 1 : 1, total flow rate: 10 mL min^{-1}, catalyst 0.094 g, reaction time 30 min, 300 W Xe lamp.

Table S5. The contents of oxygen vacancy and lattice oxygen in 1% Rh_2O_3/Ga_2O_3, 1% Rh/Ga_2O_{3-x}, 1% Rh_2O_3/ZnO, 1% Rh/ZnO_{1-x} and 1% Rh_2O_3/ZrO_2, 1% Rh/ZrO_2 catalysts.

Catalysts	Oxygen vacancy	Lattice oxygen
1% Rh_2O_3/Ga_2O_3	18.5%	81.5%
1% Rh/Ga_2O_{3-x}	25.3%	74.7%
1% Rh_2O_3/ZnO	13.1%	86.9%
1% Rh/ZnO_{1-x}	15.6%	84.4%
1% Rh_2O_3/ZrO_2	29.3%	70.7%
1% Rh/ZrO_2	30.5%	69.5%

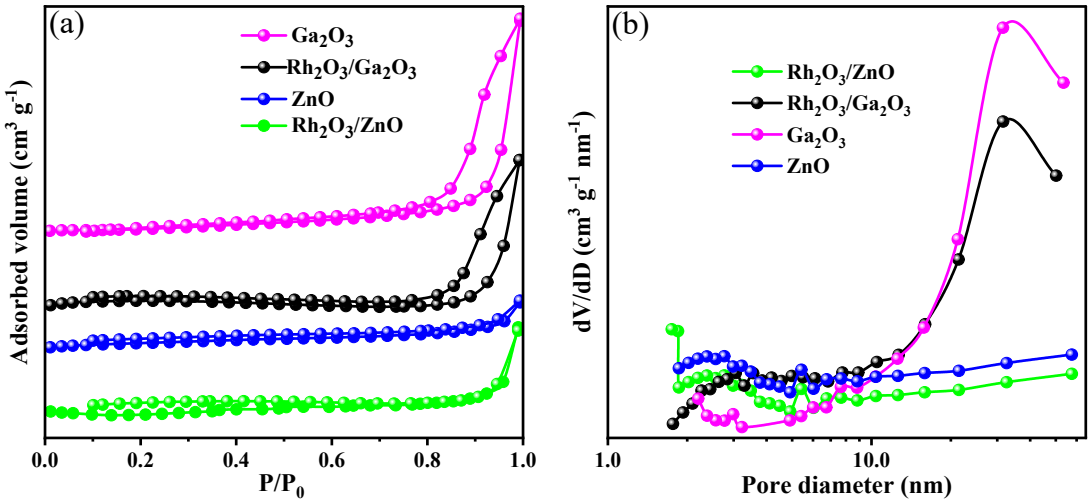

Figure S1. (a) N_2 adsorption-desorption isotherms and (b) pore size distribution of Ga_2O_3, 1% Rh_2O_3/Ga_2O_3, ZnO, and 1% Rh_2O_3/ZnO.

Note 1: All samples have the same N_2 adsorption-desorption isotherms with the IV type isotherm in IUPAC classification and observed with a loop ring of type H_3.[11] For Rh_2O_3/ZnO catalysts, no saturation adsorption platforms appear, indicating irregular mesopore structures of the samples.[12] BET surface area was measured to be 3.9, 4.6, 4.3, and 1.5 $m^2\ g^{-1}$ for Ga_2O_3, 1% Rh_2O_3/Ga_2O_3, ZnO, and 1% Rh_2O_3/ZnO, respectively.

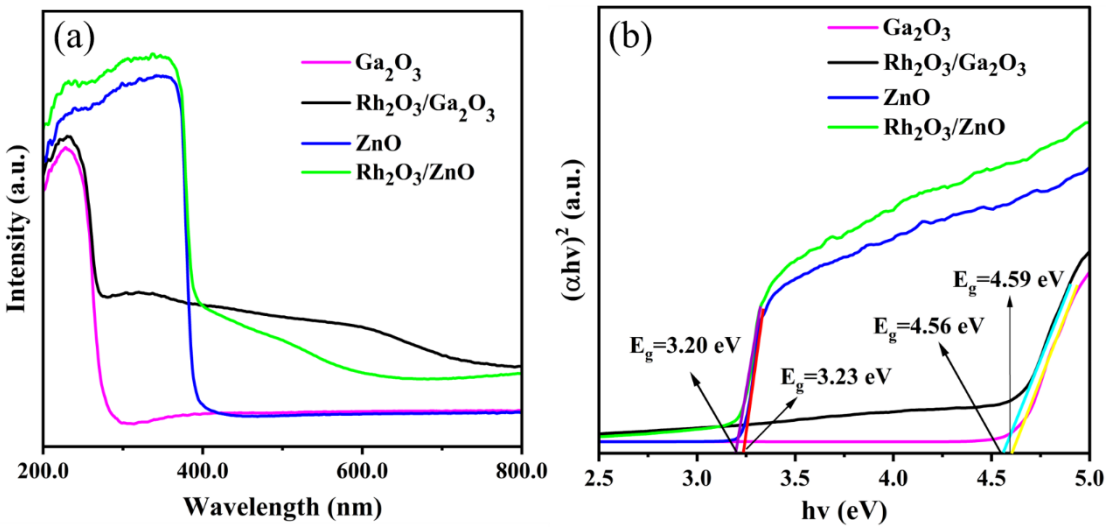

Figure S2. (a) UV-vis spectra and (b) band gap of Ga_2O_3, ZnO, 1% Rh_2O_3/Ga_2O_3, and 1% Rh_2O_3/ZnO.

Note 2: The band edges of pristine ZnO and β-Ga_2O_3 were 290 and 400 nm, corresponding to 3.23 and 4.59 eV bandgap, respectively (**Fig. S2b**). But Rh_2O_3 NPs enhanced the light absorption ability of 1% Rh_2O_3/Ga_2O_3 and 1% Rh_2O_3/ZnO, especially in the visible light range (400–800 nm) without obviously changing their band gaps.

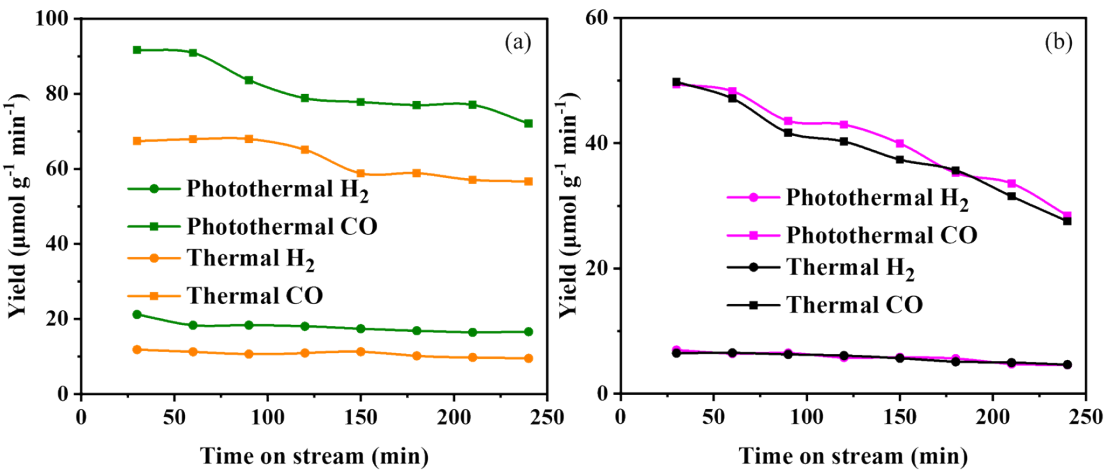

Figure S3. H_2 and CO yield on DRM reaction: (a) 1% Rh/Ga_2O_{3-x} and (b) 1% Rh/ZnO_{1-}

$_x$. Reaction conditions: 500 °C, CH_4 : CO_2 = 1 : 1, total flow rate: 10 mL min^{-1}, 0.094 g of catalyst, with or without visible light irradiation (300 W Xe lamp).

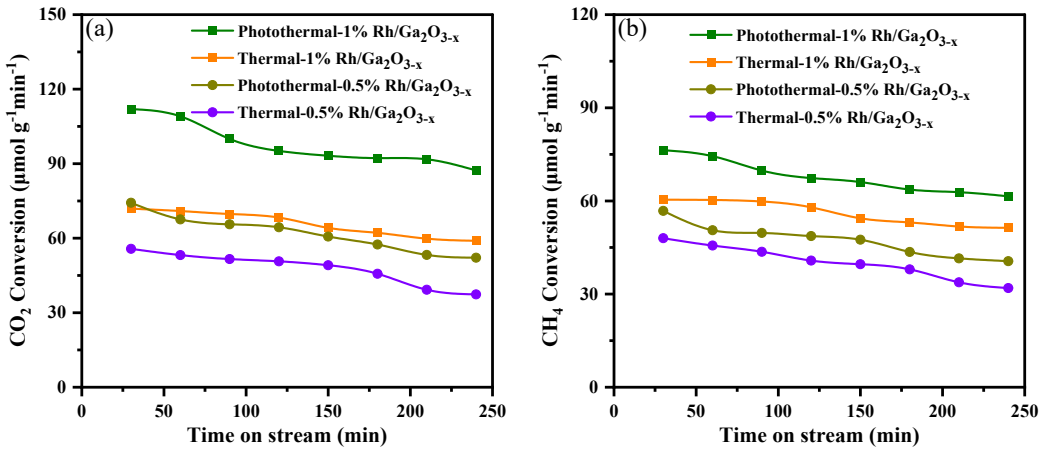

Figure S4. DRM catalytic performances over 1% Rh/Ga_2O_{3-x} and 0.5% Rh/Ga_2O_{3-x} : (a) CH_4 conversion and (b) CO_2 conversion. Reaction conditions: 500 °C, CH_4 : CO_2 = 1 : 1, total flow rate: 10 mL min^{-1}, 0.094 g of catalyst, with or without visible light irradiation (300 W Xe lamp).

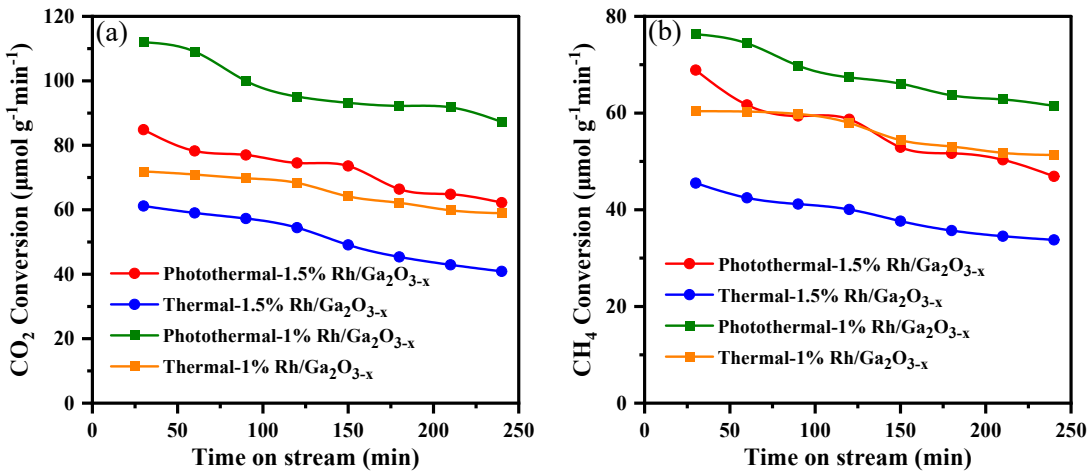

Figure S5. DRM catalytic performances over 1% Rh/Ga_2O_{3-x} and 1.5% Rh/Ga_2O_{3-x} :

(a) CH_4 conversion and (b) CO_2 conversion. Reaction conditions: 500 °C, CH_4 : CO_2 = 1 : 1, total flow rate: 10 mL min^{-1}, 0.094 g of catalyst, with or without visible light irradiation (300 W Xe lamp).

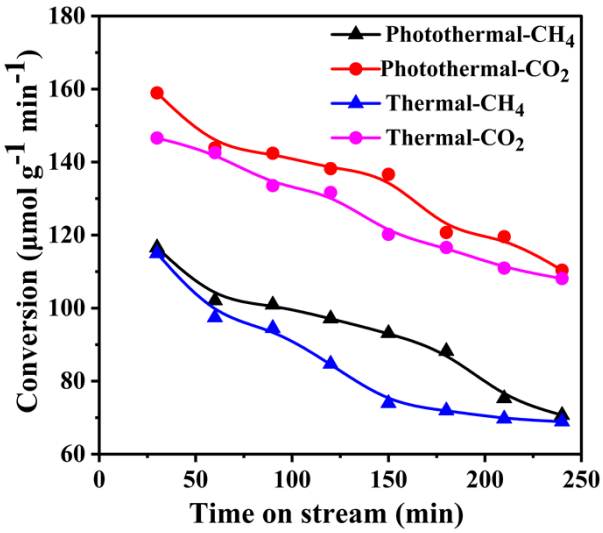

Figure S6. DRM catalytic performances over 1% Ru/Ga_2O_{3-x}: CH_4 and CO_2 conversion. Reaction conditions: 500 °C, CH_4 : CO_2 = 1 : 1, total flow rate: 10 mL min^{-1}, 0.094 g of catalyst, with or without visible light irradiation (300 W Xe lamp).

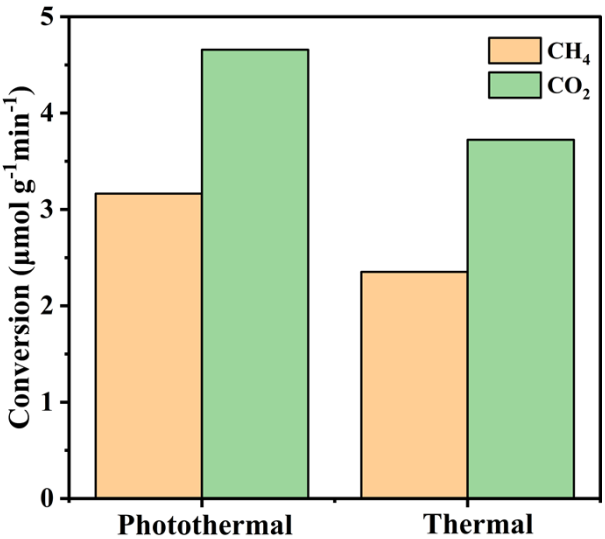

Figure S7. DRM catalytic performances over 1% Pd/Ga_2O_{3-x}. Reaction conditions: 500

°C, CH_4 : CO_2 = 1 : 1, total flow rate: 10 mL min^{-1}, 0.094 g of catalyst, with or without visible light irradiation (300 W Xe lamp).

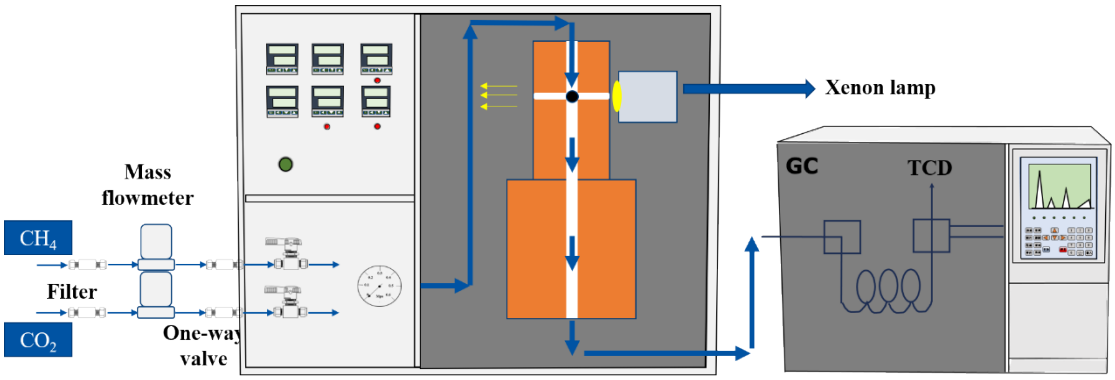

Figure S8. Fixed-bed reactor under atmospheric pressure.

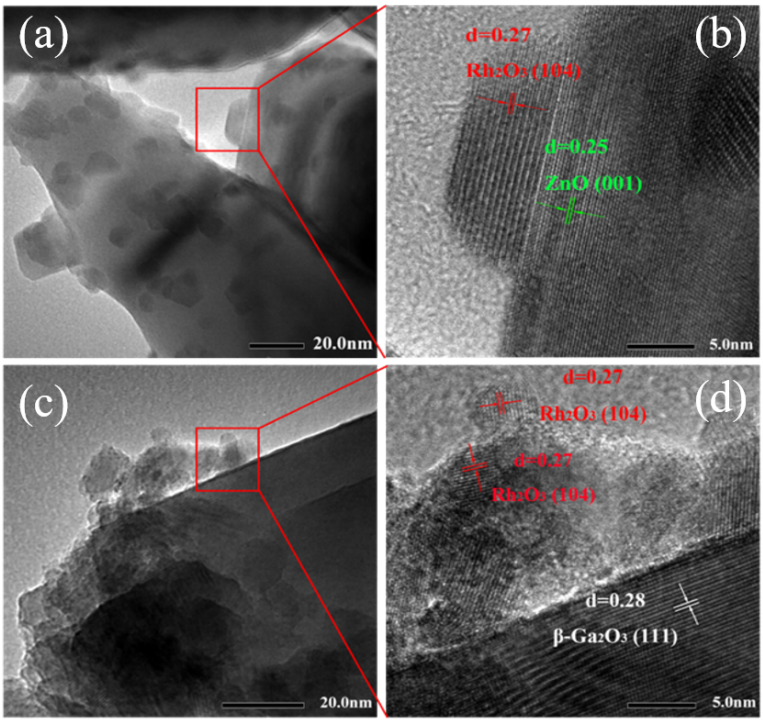

Figure S9. (a) TEM and (b) HR-TEM images of 1% Rh_2O_3/ZnO. (c) TEM and (d) HR-TEM images of 1% Rh_2O_3/Ga_2O_3.

Note 3: The morphology and crystallinity of 1% Rh_2O_3/Ga_2O_3 and 1% Rh_2O_3/ZnO samples were observed by transmission electron microscope (TEM). 1% Rh_2O_3/ZnO catalyst had a rod-like structure, and the Rh_2O_3 nanoparticles (NPs) were uniformly distributed on the ZnO surface (**Figure S9a**). The distances of clear lattice fringes were 0.27 and 0.25 nm shown on the high-resolution TEM (HRTEM) image, corresponding to Rh_2O_3 and ZnO with the good crystal structure (**Figure S9b**).[13] Similarly, it could be observed that Rh_2O_3 NPs were loaded on β-Ga_2O_3 support (d = 0.28), meaning the successful preparation of 1% Rh_2O_3/Ga_2O_3 nanocomposite (**Figure S9c** and **d**).[14, 15]

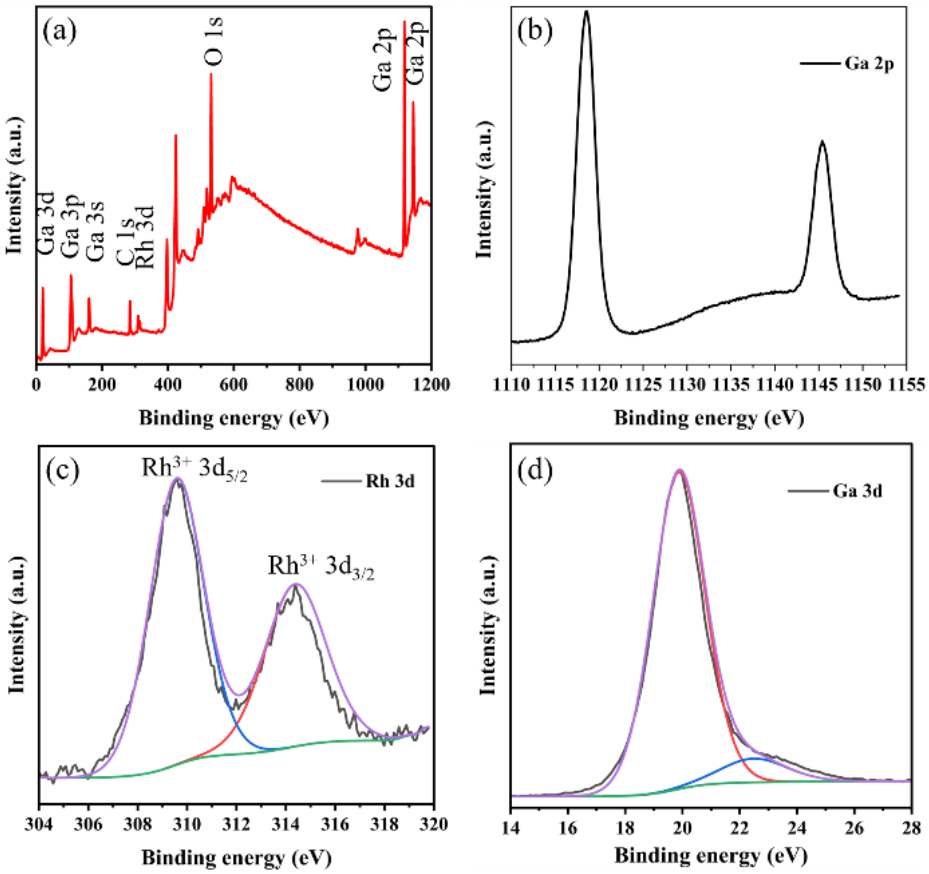

Figure S10. (a) XPS spectra of 1% Rh_2O_3/Ga_2O_3. (b) Ga 2p, (c) Rh 3d and (d) Ga 3d.

Note 4: Figure S10a revealed the coexistence of C, Ga, O, Rh, and N elements in 1%

Rh_2O_3/Ga_2O_3. The high-resolution XPS (HR-XPS) spectra of Ga 2p showed two peaks from Ga $2p_{3/2}$ and Ga $2p_{1/2}$ at 1118.53 eV and 1145.42 eV, respectively (**Figure S10b**).[16] Compared to the β-Ga_2O_3, the characteristic peaks of Ga 2p and 3d shifted slightly to lower binding energies due to the presence of Rh_2O_3.[17] Rh 3d spectra in 1% Rh_2O_3/Ga_2O_3 samples contained two peaks at 309.58 eV and 314.42 eV that can be assigned to Rh $3d_{5/2}$ and Rh $3d_{3/2}$ (**Figure S10c**).[18–19] And a peak of Ga 3d at 19.86 eV, which was attributed to Ga^{3+}, was observed in 1% Rh_2O_3/Ga_2O_3, representing the Ga–O bonding (**Figure S10d**).[16]

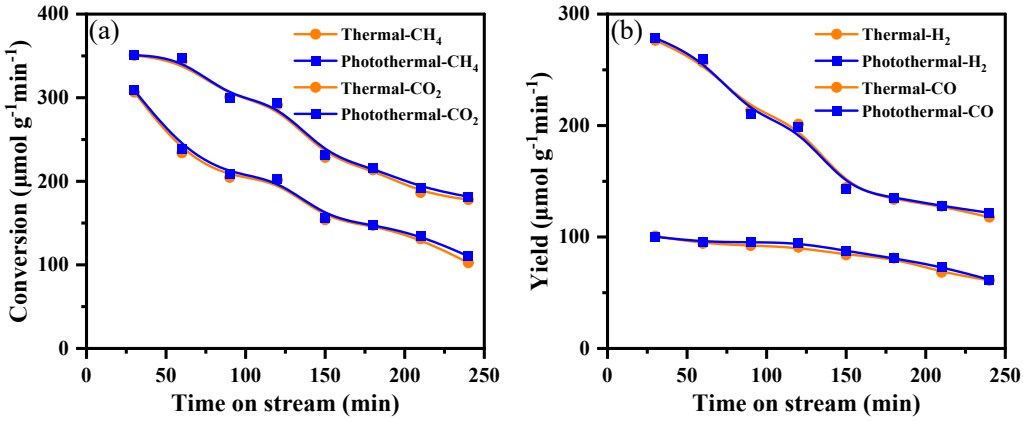

Figure S11. DRM catalytic performances over 1% Rh/ZrO_2: (a) CH_4 and CO_2 conversion and (b) H_2 and CO yield. Reaction conditions: 500 °C, CH_4 : CO_2 = 1 : 1, total flow rate: 10 mL min^{-1}, 0.094 g of catalyst, with or without visible light irradiation (300 W Xe lamp).

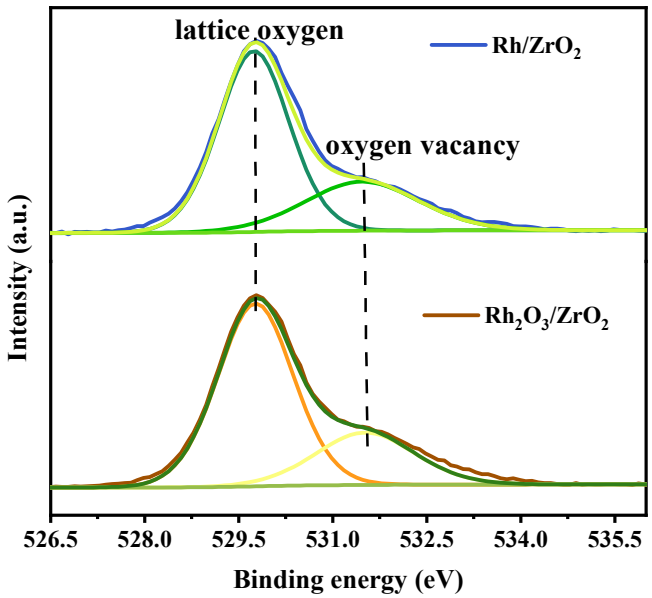

Figure S12. O1s XPS spectra of 1% Rh_2O_3/ZrO_2 and 1% Rh/ZrO_2.

Note 5: To further elucidate the role of oxygen vacancies, ZrO_2 with good stability and excellent catalytic performance was selected as the substrate to produce 1% Rh/ZrO_2 sample via the same preparation method. The DRM reactions were carried out over 1%

Rh/ZrO_2 under the same reaction conditions. The results showed that the photothermal catalytic performance of the 1% Rh/ZrO_2 catalyst was similar to thermal catalytic activity (**Figure S11**). The surface chemical properties of the catalyst were characterized by XPS (**Figure S12**), and the oxygen vacancy content of the catalyst before and after the reaction was calculated (**Table S5**). Before and after the DRM reaction, the content of oxygen vacancy in 1% Rh/ZrO_2 had only a slight variation. This indicated the enhancement effect of oxygen vacancies in the Rh/Ga_2O_{3-x} system.

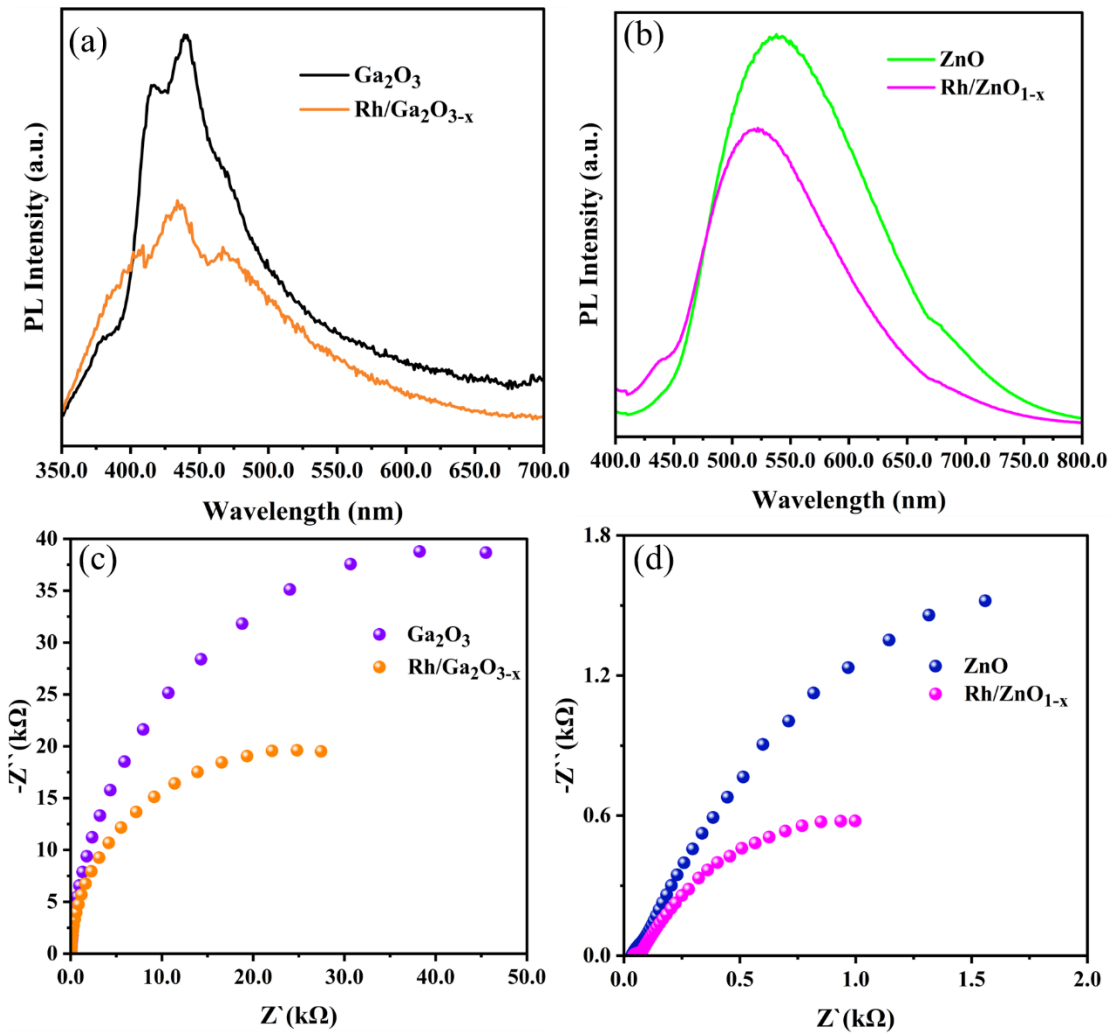

Figure S13. (a and b) PL and (c and d) EIS spectra of Ga_2O_3, 1% Rh/Ga_2O_{3-x}, ZnO and

1% Rh/ZnO_{1-x}.

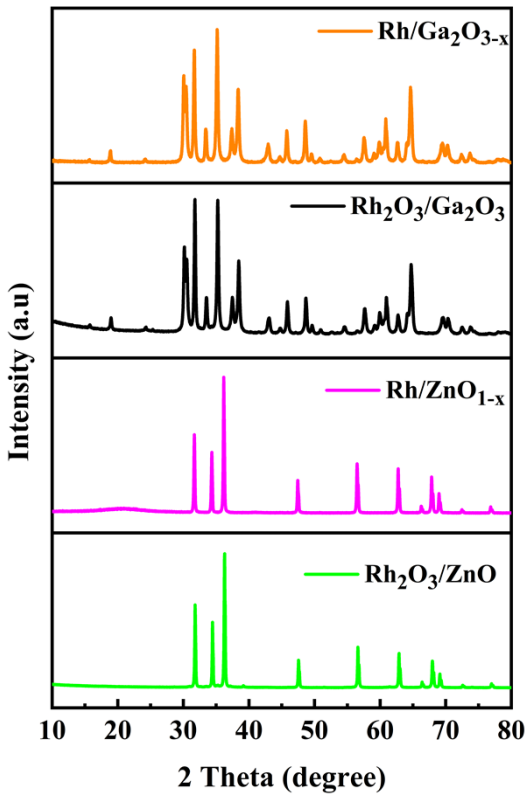

Figure S14. XRD of the fresh 1% Rh_2O_3/Ga_2O_3, 1% Rh_2O_3/ZnO the spent 1% Rh/Ga_2O_{3-x} and 1% Rh/ZnO_{1-x}.

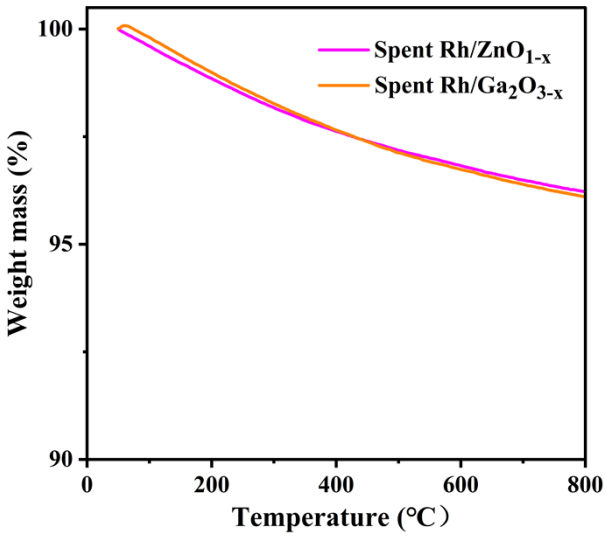

Figure S15. TG of the spent 1% Rh/Ga_2O_{3-x} and 1% Rh/ZnO_{1-x} catalysts.

Reference

1 H. Song, X. G. Meng, T. D. Dao, W. Zhou, H. M. Liu, L. Shi, H. B. Zhang, T. Nagao, T. Kako and J. H. Ye, ACS Appl. Mater. Interfaces, 2018, 10, 408–416.

2 H. M. Liu, X. G. Meng, T. D. Dao, L. Q. Liu, P. Li, G. X. Zhao, T. Nagao, L. Q. Yang and J. H. Ye, J. Mater. Chem. A, 2017, 5, 10567–10573.

3 L. A. Zhou, J. M. P. Martirez, J. Finzel, C. Zhang, D. F. Swearer, S. Tian, H. Robatjazi, M. H. Lou, L. L. Dong, L. Henderson, P. Christopher, E. A. Carter, P. Nordlander and N. J. Halas, Nat. Energy, 2020, 5, 61–70.

4 L. Sandoval-Diaz, D. Cruz, M. Vuijk, G. Ducci, M. Hävecker, W. L. Jiang, M. Plodinec, A. Hammud, D. Ivanov, T. Götsch, K. Reuter, R. Schlögl, C. Scheurer, A. Knop-Gericke and T. Lunkenbein, Nat. Catal., 2024, DOI: 10.1038/s41929-023-01090-4.

5 H. M. Liu, T. D. Dao, L. Q. Liu, X. G. Meng, T. Nagaoa and J. H. Ye, Appl. Catal. B Environ., 2017, 209, 183–189.

6 H. M. Liu, X. G. Meng, T. D. Dao, H. B. Zhang, P. Li, K. Chang, T. Wang, M. Li, T. Nagao and J. H. Ye, Angew. Chem. Int. Ed., 2015, 54, 11545–11549.

7 P. Ferreira-Aparicio, A. Guerrero-Ruiz and I. Rodrıguez-Ramos, Appl. Catal. A Gen., 1998, 170, 177–187.

8 A. I. Paksoy, B. S. Caglayan and A. E. Aksoylu, Appl. Catal. B Environ., 2015, 168, 164–174.

9 H. M. Liu, M. Li, T. D. Dao, Y. Y. Liu, W. Zhou, L. Q. Liu, X. G. Meng, T. Nagao and J. H. Ye, Nano Energy, 2016, 26, 398–404.

10 S. Shoji, X. B. Peng, A. Yamaguchi, R. Watanabe, C. Fukuhara, Y. Cho, T. Yamamoto, S. Matsumura, M. W. Yu, S. Ishii, T. Fujita, H. Abe and M. Miyauchi, Nat. Catal., 2020, 3, 148–153.

11 S. A. R. Ahmadi, M. R. Kalaee, O. Moradi, F. Nosratinia and M. Abdouss, J. Mol. Struct., 2022, 1251, 132013.

12 Y. Wang, J. Zhao, T. F. Wang, Y. X. Li, X. Y. Li, J. Yin and C. Y. Wang, J. Catal., 2016, 337, 293–302.

13 G. Lin, Z. Zhang, Q. Ju, T. Wu, C. U. Segre, W. Chen, H. Peng, H. Zhang, Q. Liu, Z. Liu, Y. Zhang, S. Kong, Y. Mao, W. Zhao, K. Suenaga, F. Huang and J. Wang, Nat. commun., 2023, 14, 280.

14 M. L. Guo, W. Q. Jiang, J. C. Ding and J. Lu, Fuel, 2022, 315, 123254.

15 A. Staerz, T. H. Kim, J. H. Lee, U. Weimar and N. Barsan, J. Phys. Chem. C, 2017, 121, 24701–24706.

16 J. P. Wei, J. Yang, Z. H. Wen, J. Dai, Y. Li and B. H. Yao, Rsc Advances, 2017, 7, 37508–37521.

17 N. Ojha, A. K. Metya and S. Kumar, Appl. Surf. Sci., 2022, 580, 152315.

18 P. K. L. Tran, D. T. Tran, D. Malhotra, S. Prabhakaran, D. Kim, N. H. Kim and J. H. Lee, Small, 2021, 17, 2103826.

19 M. Kurnatowska, M. E. Schuster, W. Mista and L. Kepinski, Chemcatchem, 2014, 6, 3125–3131.